

Article

Investigation of the Microstructure, Optical, Electrical and Nanomechanical Properties of ZnOx Thin Films Deposited by Magnetron Sputtering

Michał Mazur ^{1,*}, Agata Obstarczyk ¹, Witold Posadowski ¹, Jarosław Domaradzki ¹, Szymon Kiełczawa ¹, Artur Wiatrowski ¹, Damian Wojcieszak ¹, Małgorzata Kalisz ², Marcin Grobelny ³ and Jan Szmidt ⁴

- ¹ Faculty of Electronics, Photonics and Microsystems, Wrocław University of Science and Technology, Janiszewskiego 11/17, 50-372 Wrocław, Poland
- ² Faculty of Engineering and Economics, Ignacy Mościcki University of Applied Sciences in Ciechanów, Narutowicza 9, 06-400 Ciechanów, Poland
- ³ Faculty of Technical and Social Sciences, Ignacy Mościcki University of Applied Sciences in Ciechanów, Warszawska 52, 06-500 Mława, Poland
- ⁴ Institute of Microelectronics and Optoelectronics, Warsaw University of Technology, Koszykowa 75, 00-662 Warsaw, Poland
- * Correspondence: michal.mazur@pwr.edu.pl



Citation: Mazur, M.; Obstarczyk, A.; Posadowski, W.; Domaradzki, J.; Kiełczawa, S.; Wiatrowski, A.; Wojcieszak, D.; Kalisz, M.; Grobelny, M.; Szmidt, J. Investigation of the Microstructure, Optical, Electrical and Nanomechanical Properties of ZnOx Thin Films Deposited by Magnetron Sputtering. *Materials* **2022**, *15*, 6551. <https://doi.org/10.3390/ma15196551>

Academic Editors: Gueorgui Gueorguiev and Anna Tyszka-Zawadzka

Received: 25 August 2022
Accepted: 14 September 2022
Published: 21 September 2022

Publisher's Note: MDPI stays neutral with regard to jurisdictional claims in published maps and institutional affiliations.



Copyright: © 2022 by the authors. Licensee MDPI, Basel, Switzerland. This article is an open access article distributed under the terms and conditions of the Creative Commons Attribution (CC BY) license (<https://creativecommons.org/licenses/by/4.0/>).

Abstract: The paper presents the results of an investigation of the influence of technological parameters on the microstructure, optical, electrical and nanomechanical properties of zinc oxide coatings prepared using the pulsed reactive magnetron sputtering method. Three sets of ZnOx thin films were deposited in metallic, shallow dielectric and deep dielectric sputtering modes. Structural investigations showed that thin films deposited in the metallic mode were nanocrystalline with mixed hexagonal phases of metallic zinc and zinc oxide with crystallite size of 9.1 and 6.0 nm, respectively. On the contrary, the coatings deposited in both dielectric modes had a nanocrystalline ZnO structure with an average crystallite size smaller than 10 nm. Moreover, coatings deposited in the dielectric modes had an average transmission of 84% in the visible wavelength range, while thin films deposited in the metallic mode were opaque. Measurements of electrical properties revealed that the resistivity of as-deposited thin films was in the range of 10^{-4} Ωcm to 10^8 Ωcm. Coatings deposited in the metallic mode had the lowest hardness of 2.2 GPa and the worst scratch resistance among all sputtered coatings, whereas the best mechanical properties were obtained for the film sputtered in the deep dielectric mode. The obtained hardness of 11.5 GPa is one of the highest reported to date in the literature for undoped ZnO.

Keywords: ZnO thin film; pulsed reactive magnetron sputtering; hardness; scratch resistance; optical properties; electrical properties; structural properties

1. Introduction

Zinc oxide (ZnO) and its compounds are now among the materials widely used in microelectronics. Due to the depletion of indium resources, transparent ZnO is an attractive semiconducting oxide that, with appropriate modifications, is a promising candidate for replacing indium-tin oxide thin films, commonly used in microelectronics for the fabrication of, among other things, transparent electrodes [1]. Zinc oxide is a wide band-gap semiconductor of the II-VI semiconductor group that has several favorable properties, such as good transparency in the wide wavelength range, high electron mobility, wide and direct band gap (3.37 eV), high exciton binding energy (60 meV) and strong room temperature luminescence [2–5]. Moreover, ZnO is generally an n-type transparent oxide semiconducting material [4]. However, an additional advantage is the possibility of the preparation of p-type transparent conductive coatings using in situ doping of ZnO during its deposition [6]. The form type and dimensions of ZnO nanostructures have a strong

impact on its features as well [7–9]. All of the listed properties and additionally the high thermal and mechanical stability at room temperature make it attractive for potential use in electronics, optoelectronics and laser technology [10]. ZnO has found applications in the manufacturing of devices such as varistors, gas sensors, transparent electrodes for thin-film transistors and solar cells. The other emerging applications include light emitting diodes (LEDs), laser diodes (LDs) and light detectors [1,3,11]. ZnO is often used for the preparation of various junctions and heterostructures [12–15]. The piezoelectric and pyroelectric properties of ZnO make it possible to use in sensors, converters, energy generators and photocatalysts in hydrogen production [11,16]. Due to its hardness, stiffness and piezoelectric constant, it is an important material in the ceramics industry, while its low toxicity, biocompatibility and biodegradability result in increased interest for its application in biomedicine and in ecological systems [10,17].

ZnO thin films can be prepared on an industrial scale using many methods [3,10,18,19]. One of them is magnetron sputtering, which ensures a stable and high-efficiency deposition process and provides the possibility of obtaining coatings on large-scale substrates. Moreover, in this method, the properties of the ZnO film can be controlled by changing the sputtering conditions such as substrate temperature, deposition time, pressure and power [3]. There are many types of magnetron sputtering methods, including direct current (DC), radio frequency (RF) and high-power impulse magnetron sputtering (HiPIMS), among others. Radio frequency magnetron sputtering RF MS (13.56 MHz, 27 MHz) allows the sputtering of nonconductive and conductive materials. In the case of the deposition of non-conducting ZnO, a metallic Zn target is usually sputtered in an oxygen atmosphere. In each case, partial pressure is an important process parameter, and usually the target power density does not exceed 10 W/cm^2 [2,3,20–32]. Controlling the level of oxygen doping during the RF process allows one to control the stoichiometry of the deposited films. It is also possible to obtain Zn oxide coatings using DC MS by sputtering the conductive target. In most cases, this forces the use of targets made of metallic Zn material. As in the case of RF MS, the target power density also does not exceed 10 W/cm^2 [33–43]. Recently, a lot of attention has been focused on high-power impulse magnetron sputtering [44–46]. In this method, the target is sputtered with very high and short current pulses in which duration is on the order of a dozen or several dozen microseconds. Current waveforms are modulated at a frequency of several kHz. However, it is worth highlighting that the average power released in the target is similar to standard DC and RF MS processes (although the sputtering efficiency is relatively smaller). In turn, with the HiPIMS method, mechanical properties such as hardness or optical properties of deposited films can be enhanced due to phenomena accompanying the initiation and pulse suppression.

In the present paper, the influence of the oxygen content in the sputtering atmosphere on various properties of zinc oxide thin films was discussed. It was found that the change in the sputtering mode had a significant effect on the microstructure, morphology, electrical, optical and mechanical properties of the sputtered ZnOx thin films. It is also worth noting that the hardness determined for the ZnO thin film deposited in the deep dielectric mode has been one of the highest reported in the literature and the coating had excellent scratch resistance.

2. Materials and Methods

For the deposition of ZnOx, thin films' reactive pulsed magnetron sputtering process of metallic zinc targets was used. Deposition processes were carried out in an NP-500 vacuum stand setup (Bolesławiec, Poland) equipped with a pumping system (Tepro, Koszalin, Poland) consisting of diffusion (2000 L/s) and rotary (30 m³/h) pumps. The final pressure obtained with a vacuum set was equal to $2 \cdot 10^{-5}$ Torr. Each sputtering process was carried out in the atmosphere containing a mixture of argon and oxygen gases (Ar:O₂), and the working pressure of the gas atmosphere was changed in the range from 1×10^{-3} to 8×10^{-3} Torr. Circular WMK-100 magnetron (handmade) was used, which was equipped with a high purity circular Zn (99.999%) disc with a diameter of 100 mm and a thickness

of 9 mm. The used magnetron offers the possibility of conducting processes with a very high power released in the sputtered target, which is directly related to the efficiency of the deposition processes of thin films. The magnetron was powered using an MSS-10kW power supply unit (Dora Power System—PWM type, Wilczyce, Poland). A distinctive feature of this power supply unit is the possibility of in situ observations of sputtering processes by monitoring its parameters [47]. In particular, the most important parameter is called the circulating power (the term introduced by the Dora Power System manufacturer), reflecting changes in a load impedance. In turn, impedance is determined by specific technological conditions of the sputtering process and is affected, for example, by the change of the: (1) type and composition of the working gas, (2) target thickness, and (3) surface of the sputtered material (e.g., coverage of the target with a reactive compound formed in the presence of chemically active gases). This is an original feature of the DPS power supply that can be used to control the deposition process. Thin films were deposited on fused silica (SiO₂), silicon (Si) and alumina substrates containing interdigitated electrodes designed for electrical measurements. The thickness of the deposited ZnOx thin films was assessed with the use of the Taylor-Hobson CCI Lite optical profilometer (Leicester, UK).

The microstructure was studied by X-ray diffraction in grazing incidence mode (GIXRD) using a Panalytical X'Pert Pro diffractometer (Panalytical, Malvern, UK) equipped with the Cu K α X-ray source with a wavelength of 1.5406 Å. Crystallite size analysis was performed according to the Debye-Scherrer equation [48] with the aid of MDI JADE 5.0 software. The surface morphology and cross section of as-prepared coatings were investigated using a FEI Helios Xe-PFIB field-emission scanning electron microscope (FE-SEM) equipped with EDAX energy dispersive spectroscopy (EDS) detector (Hillsboro, OR, USA).

Optical measurements were conducted in the wavelength range of 300–1000 nm using an Ocean Optics QE65000 spectrophotometer and a coupled deuterium-halogen light source (Ocean Optics, Largo, FL, USA). The measurements of transparent ZnOx thin films were completed by evaluating the fundamental absorption edge ($\lambda_{\text{cut-off}}$). The refractive index (n) and extinction coefficient (k) spectral characteristics of the transparent films were determined by the reverse engineering method using the FTG FilmStar software (Princeton, NJ, USA) employing a generalized Cauchy model for materials with $k > 0$.

The resistivity of the deposited coatings was determined using current-voltage characteristics measured at room temperature in a dark shielded enclosure with the aid of a Keithley SCS4200 system (Keithley Instruments LLC, Cleveland, OH, USA) and a M100 Cascade Microtech probe station (Cascade Microtech, Beaverton, OR, USA).

The mechanical properties of prepared zinc oxide thin films were determined using a nanoindentation method with the aid of a CSM Instruments (Peseux, Switzerland) nanoindenter equipped with a diamond Vickers tip. The results were analyzed using the method proposed by Oliver and Pharr [49]. In turn, the scratch resistance of the deposited zinc oxide thin films was measured using the Bayer test and the Taber Oscillating Abrasion tester 6160 (North Towananda, NY, USA). The oscillating movement of the abrasive medium, that is, 6/9 silica sand, simulates the everyday wear of the measured coating. The resistance to abrasion was determined using the oscillating sand test described in ASTM F735 [50]. The movement distance of the sand tray was equal to 100 mm at a speed of 300 strokes per minute. The surface topography of the deposited thin films was examined before and after the scratch test using a TalySurf CCI Lite Taylor-Hobson optical profiler and an Olympus BX51 optical microscope (Bartlett, TN, USA). As an indicator of scratch resistance (hereinafter referred to as *SRes*), a comparison was made of the mean square root height (*Sq*) measured before and after the abrasion test as in Equation (1):

$$SRes = \frac{Sq_{\text{before}}}{Sq_{\text{after}}} \times 100\% \quad (1)$$

where Sq_{before} is the mean square root height before abrasion test and Sq_{after} is the mean square root height after abrasion test.

It can be estimated that the closer the $SRes$ is to 100%, the more resistant the coating is to scratching due to the negligible change in the roughness of its surface.

3. Results and Discussion

3.1. Deposition of ZnOx Thin Films

Preliminary experiments performed by the authors have shown that the relation between the effective power P_E (proportional to thin film deposition rate) and circulating power P_C (as an indicator of the target surface condition) of the power supply (P_E/P_C) measured during sputtering in the argon atmosphere allows us to calibrate and scale magnetron sputtering processes in the atmosphere of the argon and oxygen mixture. The sputtering of the Zn target in an Ar atmosphere with effective power of $P_E = 1$ kW (target power density of ca. 12 W/cm^2) and substrate target distance (d_{S-T}) equal to 130 mm resulted in the Zn film deposition rate equal to 300 nm/min. In turn, P_E equal to 6.1 kW (target power density of ca. 78 W/cm^2) resulted in a deposition rate of Zn films of ca. 2000 nm/min. Additionally, changing the d_{S-T} to 90 mm and providing the P_E of 1.6 kW (target power density of approximately 20 W/cm^2) resulted in a decrease in the deposition rate to approximately 800 nm/min.

In this paper, ZnOx thin films were deposited by sputtering a Zn target in pure oxygen and also in the atmosphere of the argon and oxygen mixture. In each process, the composition of the sputtering atmosphere and power supplying target (process parameters) were changed. The dependence of the effective power on the circulating power P_E/P_C (Figure 1) measured during sputtering in pure argon and pure oxygen allowed us to determine the boundary electrical parameters of the power supply when the target surface was still metallic (metallic mode) or it was already fully oxidized (dielectric mode). The deposition of thin films using reactive magnetron sputtering required the determination of the most favorable technological conditions of the process. The most important requirements are the composition of the working gas and the total pressure of the gas mixture during the sputtering process. The nature of the reactive sputtering process forced the determination of certain procedures while setting the gas level, which was possible due to the in situ observation of the sputtering process based on the value of circulating power.

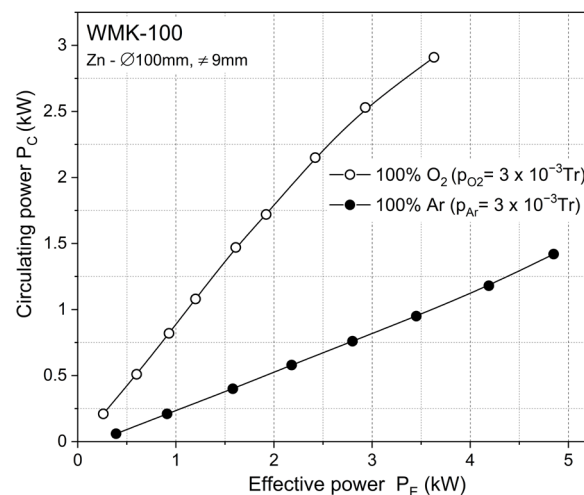


Figure 1. Dependence between effective power (P_E) and circulating power (P_C) measured during the sputtering of Zn target in Ar (pure metallic target surface—metallic mode) and O₂ atmosphere (fully oxidized target surface—dielectric mode).

Observation of the circulating power gives information on the surface condition of the target during reactive sputtering. Covering a sputtered target with dielectric compound, i.e., its oxidation, changes the electrical conditions of its surface because the secondary electron emission factors from the dielectric layer are, on average, one order larger than

those for a pure metal. The relationship between the DPS power supply (effective power versus circulating power) and the surface of the sputtered material mirrors the target surface status (Figure 2).

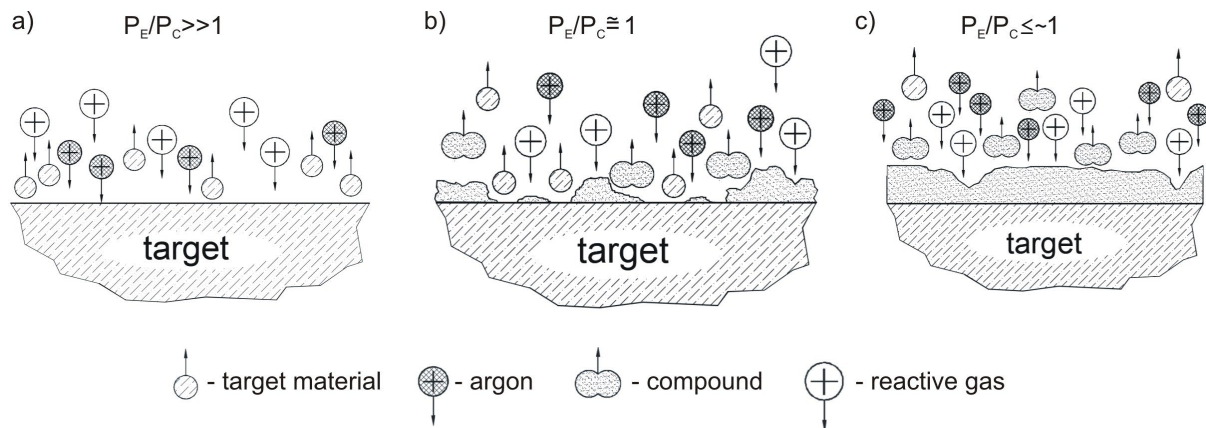


Figure 2. Schematic view of the formation of the reactive compound on the surface of the sputtered material as a function of the electrical parameters of the DPS power supply: (a) metallic mode (Ar atmosphere)—target surface not covered by the compound; (b) shallow dielectric mode—target surface partially covered by a compound; (c) deep dielectric mode (O_2 atmosphere)—target surface completely coated with the compound.

In particular, the P_E/P_C value is an important parameter of the reactive sputtering process, providing information about the target surface coverage (depending on the magnetron sputtering mode during the deposition process). The formation of a reactive compound on the metallic target changes the physicochemical properties of the surface, leading to a significant reduction in the deposition rate. The sputtering yield of a dielectric compound is often an order of magnitude lower than that of metals. The increase in the circulating power value always clearly indicates the technological point when the deposited dielectric thin films are transparent, hard and exhibit good adhesion to the substrate.

The hysteresis effect of the reactive magnetron sputtering process is the result of phenomena occurring on the surface of the sputtered material. The metallic target is an efficient source of sputtered metal (zinc) vapor. When the target surface is covered with zinc oxide, the sputtering efficiency significantly decreases. As a result, there is ambiguity in the sputtering conditions of the target, whose surface may be unstable (balance between the formation of the compound and its etching from the target). This is due to the hysteresis phenomenon that occurs if the sputtering parameters, such as target power and reactive gas flow, are changed. Figure 3 presents the hysteresis phenomenon of the dependence of $P_C = f(O_2)$ for sputtering processes with an effective power equal to 1.6 kW. It can be concluded that the oxide layer on the target starts to grow at $p_{O_2} = \sim 5 \times 10^{-3}$ Torr, and the point (c2) describes the conditions under which the Zn target is covered by the dielectric ZnO_x compound. The reduction of the partial pressure of oxygen does not cause an immediate return of the magnetron to the metallic mode but the gradual shift of the work point to the (c1) point, while the target is still covered with oxide. Decreasing the partial pressure of oxygen below $p_{O_2} = \sim 3 \times 10^{-3}$ Torr causes a change from oxide to metallic mode, which means that the Zn target is no longer poisoned with an oxide ((a) point). The authors named points (c1) and (c2) as the shallow dielectric mode and the deep dielectric mode, respectively. With the dynamically determined partial pressure of oxygen (based on the circulating power value) at a constant argon pressure, the characteristics of $P_C = f(p_{O_2})$ were measured for an effective power equal to 1.6 kW. As can be seen in Figure 3, the hysteresis effect was observed in the entire effective power range.

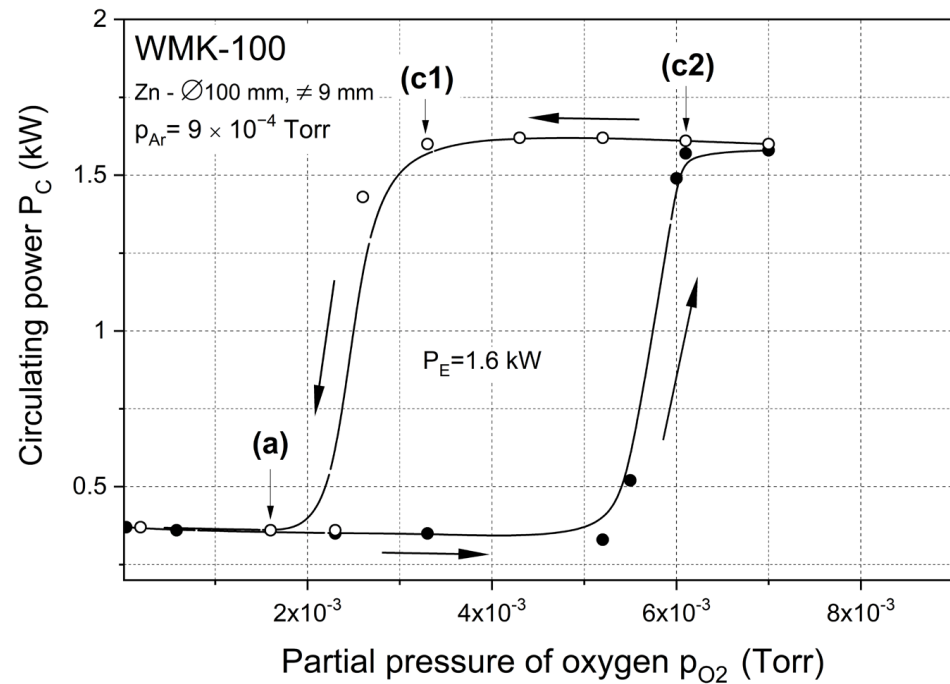


Figure 3. Influence of the partial pressure of oxygen on the value of the circulating power during the reactive sputtering of the Zn target in the mixed Ar and O₂ atmosphere at $P_E = 1.6$ kW.

The sputtering efficiency of ZnOx films was measured for coatings deposited at an effective power of 1.6 kW (Figure 4). As the oxygen content in the mixed Ar and O₂ atmosphere increased, from a certain percentage of oxygen in the Ar:O₂ atmosphere, a rapid decrease in the deposition rate of thin films was observed with a simultaneous rapid increase in the circulating power. Under these technological conditions, the Zn target was completely oxidized.

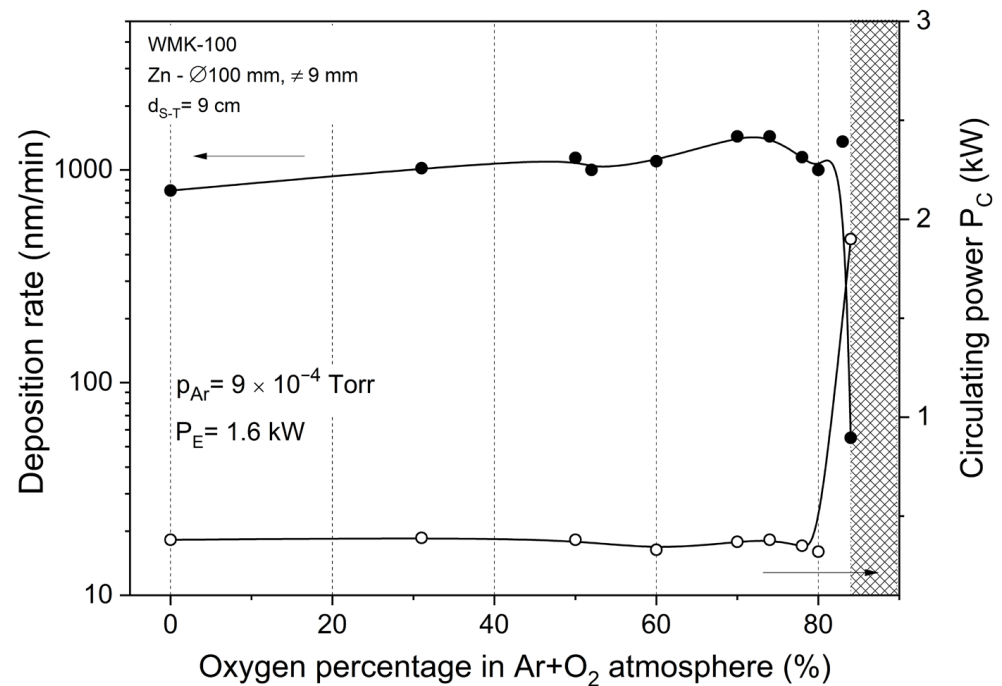


Figure 4. Influence of the percentage of oxygen content in the Ar:O₂ atmosphere on the deposition rate of the ZnOx films and circulating power.

Conductive and opaque thin films were obtained despite the fact that all sputtering processes were carried out at a relatively high concentration of O₂ in the Ar:O₂ atmosphere. From a certain oxygen concentration in the sputtering atmosphere, the deposited films were transparent and exhibited good adhesion to the substrate. The shaded area marked in Figure 4 identifies a transparent zinc oxide film with good adhesion to the substrate. At the set target power level, the oxide coatings were sputtered with a deposition rate of ~20 nm/min. The gradual increase of the oxygen content in the sputtering process caused an increase in the resistivity of the deposited films (Figure 4) up to the point where they became transparent and electrically nonconductive. It was observed that when the O₂ content was greater than 85% in the Ar:O₂ atmosphere, thin films became dielectric. The percentage content of oxygen in the working atmosphere was estimated on the partial pressure basis of the values measured after the sputtering process. The determination of the limit of oxygen content in the sputtering process, simultaneously defining the metallic and dielectric modes, was consistent with the value of the circulating power during the sputtering process.

In this work, three sets of ZnOx thin films were deposited with different technological parameters. ZnOx coatings were prepared with various and dynamically determined partial pressure of oxygen. The Zn target was sputtered in three different modes: (a) metallic, (c1) shallow dielectric and (c2) deep dielectric (Figure 3). Moreover, the deposition time was also matched with the sputtering modes and was equal to 30, 300 and 480 s for metallic, shallow and deep dielectric modes, respectively. Different sputtering times were related to the deposition rate and were selected so that the thickness of the films was in the range of 500 nm. The thickness of the films deposited in the metallic mode (a) was equal to 450 nm, whereas the thickness of the coatings deposited in the shallow (c1) and deep dielectric (c2) modes was equal to 350 nm and 570 nm, respectively.

3.2. Structural Properties of ZnOx Thin Films

XRD analysis was performed to determine the structural properties of the prepared ZnOx thin films (Figure 5). It was found that the diffraction pattern obtained for coatings deposited at the (a) work point (metallic mode) revealed the coexistence of metallic and oxide hexagonal phases of Zn and ZnO. The deposited thin film was nanocrystalline with small crystallites with size equal to 9.1 and 6.0 nm for Zn and ZnO, respectively. Furthermore, the zinc oxide coatings deposited at working points (c1) and (c2) had the polycrystalline structure of the hexagonal ZnO phase with the most dominant peak occurring at $2\theta = 34^\circ$ and associated with the (002) lattice plane. The lattice planes observed for the ZnO film deposited in the deep dielectric mode (c2 work point) were more intense than for the film deposited in the shallow dielectric mode (c1 point). In the case of ZnO films deposited at the working points (c1) and (c2), the crystallite size was equal to 7.4 nm and 6.7 nm, respectively. XRD measurements performed for thin films sputtered in dielectric modes revealed a shift of the diffraction peaks related to the ZnO hexagonal phase towards a lower angle (2θ), which may indicate the presence of a tensile stress occurring in the structure. In turn, in the case of coatings sputtered in the metallic mode, there was a visible shift of the diffraction peaks related to the metallic Zn-hexagonal phase toward a higher angle, which can testify about the presence of a compression stress. The results of the XRD measurements are summarized in Table 1.

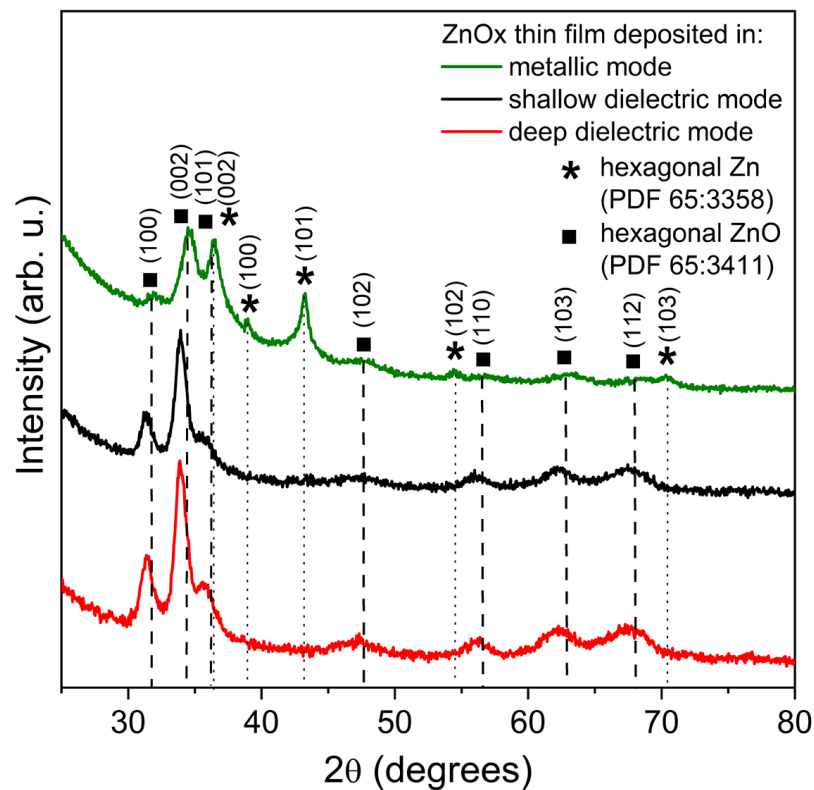


Figure 5. Diffraction patterns of ZnOx thin films deposited in metallic mode (a) work point, shallow dielectric mode (c1) work point and deep dielectric mode (c2) work point.

Table 1. Summary of XRD investigations of ZnOx thin films.

ZnOx Thin Film—Deposition Mode	Phase	(hkl)	2θ (o)	d _{hkl} (nm)	d _{PDF} (nm)	D (nm)
metallic	hexagonal-Zn	(101)	43.19	0.20927	0.20915	9.1
	hexagonal-ZnO	(002)	34.43	0.26028	0.26035	6.0
shallow dielectric	hexagonal-ZnO	(002)	34.42	0.26404	0.26035	8.7
deep dielectric	hexagonal-ZnO	(002)	34.42	0.26409	0.26035	8.1

Designations: (hkl)—set of planes, d_{hkl}—measured interplanar distance, d_{PDF}—standard interplanar distance from JCPDS card, D—crystallite size calculated according to the Scherrer's equation.

The surface and cross-section morphology of the deposited thin films at different partial pressure of oxygen p_{O2} was obtained using FE-SEM and shown in Figure 6 with thickness markers at the cross sections. It was found that the surface of the ZnOx coatings sputtered in the metallic mode was composed of spherical-shaped nanosized grains with various sizes and slight voids between them. The cross section showed that the microstructure consisted of coarse grains and that the thin film was very rough. In turn, coatings deposited in shallow and deep dielectric modes had a very smooth surface composed of homogeneously distributed nanograins with almost uniform size. The cross-sectional morphology revealed columnar growth of the coatings and the fact that a change in the sputtering mode caused densification of the thin films. Furthermore, the columnar growth started from the substrate, and the columns tended to thicken their diameter during crystal growth.

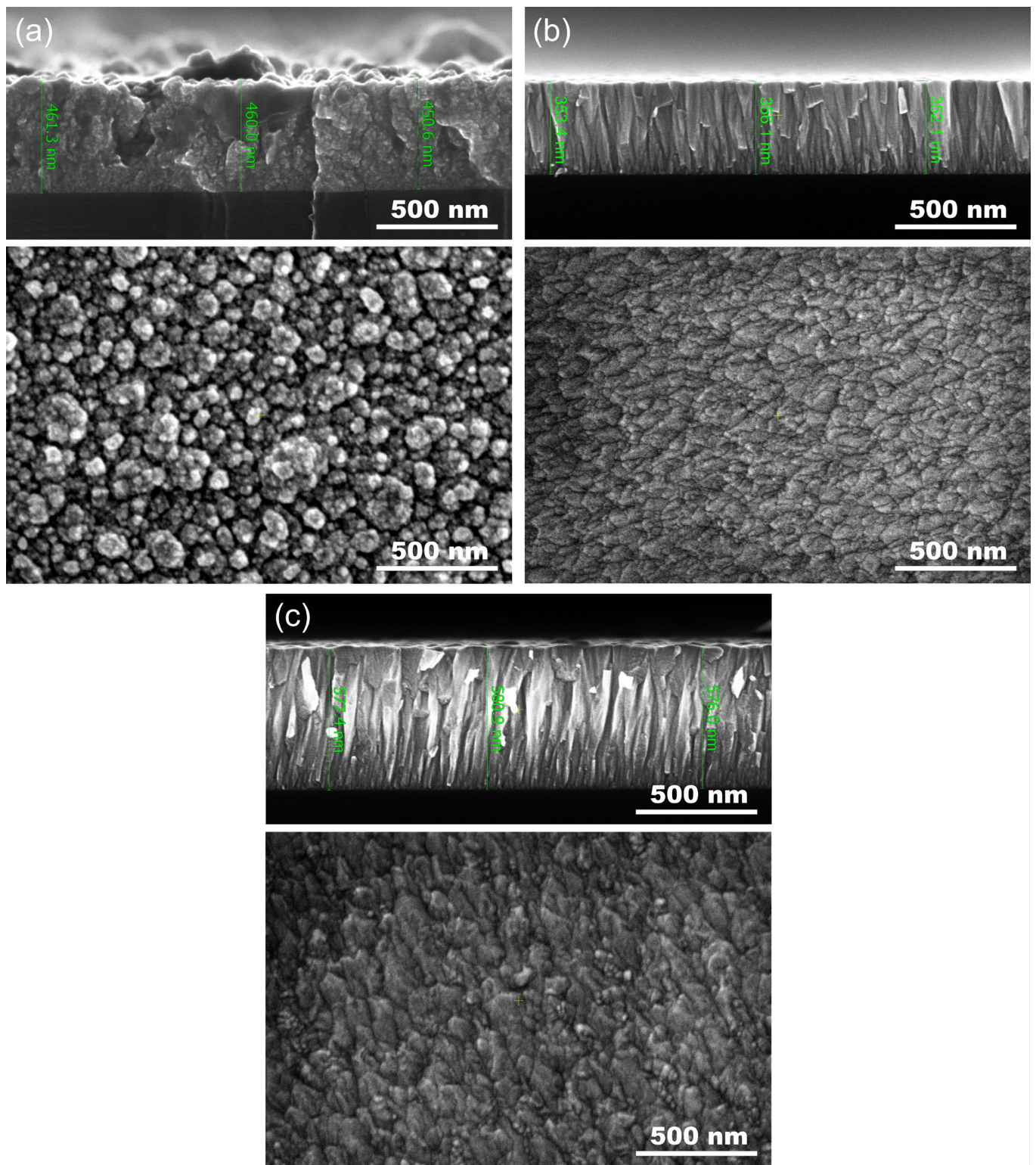


Figure 6. SEM images of ZnOx thin films deposited in modes: (a) metallic, (b) shallow dielectric and (c) deep dielectric.

Secondary electron images, elemental distribution maps of zinc and oxygen and EDS spectra taken for ZnOx thin films deposited in metallic and deep dielectric modes are shown in Figure 7. The gathered maps (Figure 7a) showed homogenous distribution of each element, i.e., Zn and O. EDS spectra (Figure 7b) showed peak lines related to Zn

($L\alpha$ line at 1.01 keV) and O ($K\alpha$ line at 0.53 keV) from the thin film and Si from substrate material ($K\alpha$ line at 1.74 keV). It is clearly seen that for the deep dielectric mode, the oxygen-related peak is much higher compared to the thin film from the metallic mode, which is understandable given the nature of both modes of the magnetron sputtering process. Furthermore, there were no other peaks that could come from other elements, which is evidence of the good purity of the deposited zinc oxide thin films.

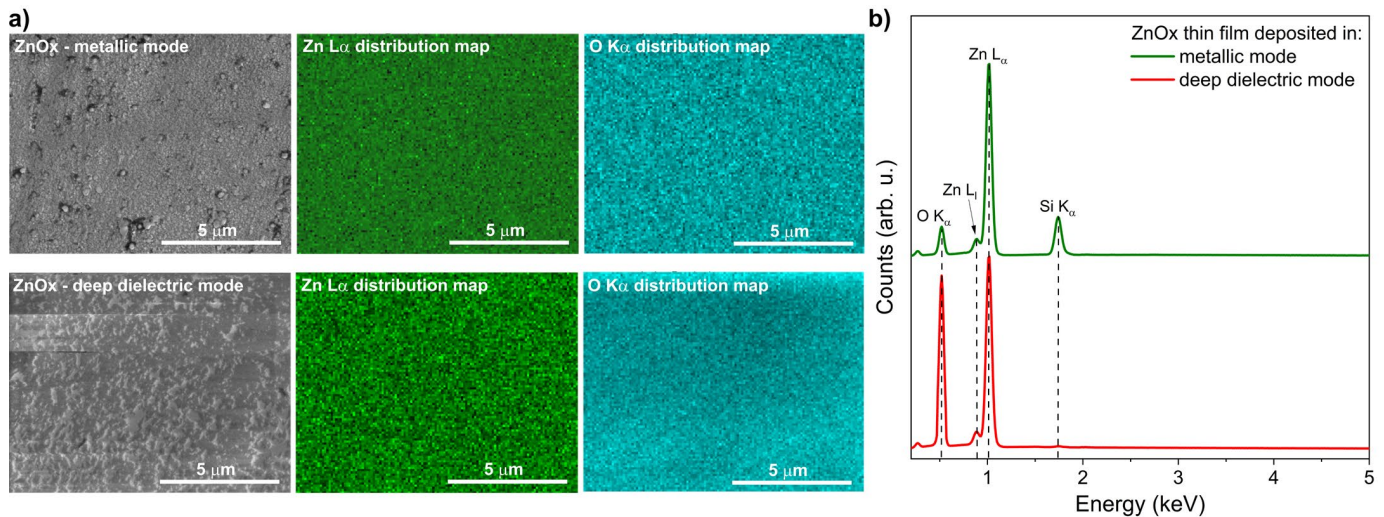


Figure 7. Results of material composition investigation: (a) elemental distribution maps and (b) EDS spectra of ZnOx thin films deposited in metallic and deep dielectric modes.

3.3. Optical Properties of ZnOx Thin Films

The optical properties of the deposited ZnOx thin films were determined based on measurements of light transmission in the wavelength range of 300–1000 nm (Figure 8a). It was found that coatings sputtered in the metallic mode were opaque in the measured wavelength range, although their microstructure consisted of both metallic Zn and oxide ZnO phases. In turn, the ZnOx films deposited in the shallow dielectric (c1) and deep dielectric (c2) modes were well transparent with an average transparency of approximately 84%. The results of the determination of the position of the fundamental absorption edge are also presented in Figure 8a. The lowest cut-off wavelength ($\lambda_{\text{cut-off}}$) was equal to 361 nm for the ZnOx film deposited in the shallow dielectric mode (c1 work point). The change in the deposition mode to (c2) work point resulted in a slight shift of the fundamental absorption edge towards a longer wavelength of 370 nm. Moreover, the optical band gap energy (E_g^{opt}) of the ZnOx thin films was calculated using the Tauc plot [51]. The optical band gap energy was estimated by extrapolating the linear portion of the curves presented in Figure 8b. In the case of ZnO films deposited in shallow dielectric and deep dielectric modes, the value of E_g^{opt} was equal to 3.30 eV and 3.25 eV, respectively.

Based on the results of the transmission characteristics (Figure 8a), with the aid of the reverse engineering method and Film Star software (v. 2.61), the refractive index (n) and the extinction coefficient (k) were calculated and plotted in Figure 9. It was found that the n at $\lambda = 550$ nm for nanocrystalline ZnOx thin films deposited in shallow and deep dielectric modes were approximately 1.97–1.98 (Figure 9a). Furthermore, the analysis of the extinction coefficient showed that the optical losses are two times higher for the ZnOx film deposited in the shallow dielectric mode for which the extinction coefficient was equal to 6.2×10^{-3} (Figure 9b). However, the obtained values of the extinction coefficient testify about very good optical properties of both coatings.

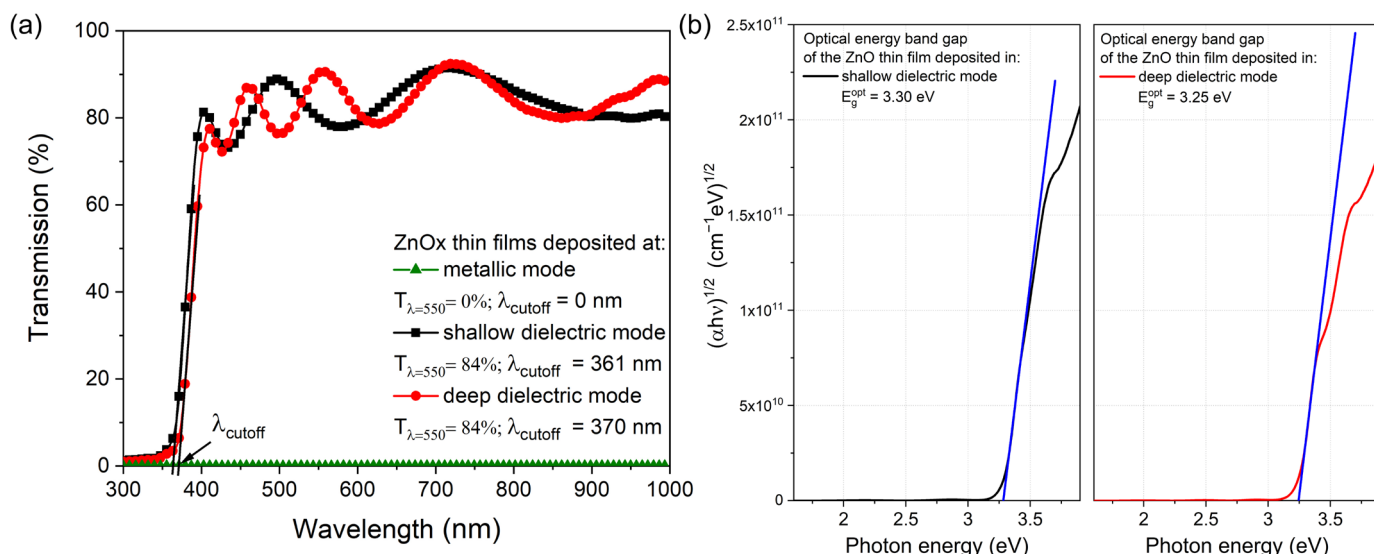


Figure 8. Transmission spectra (a) and Tauc plots (b) of transparent ZnOx thin films prepared in shallow dielectric and deep dielectric modes of magnetron sputtering.

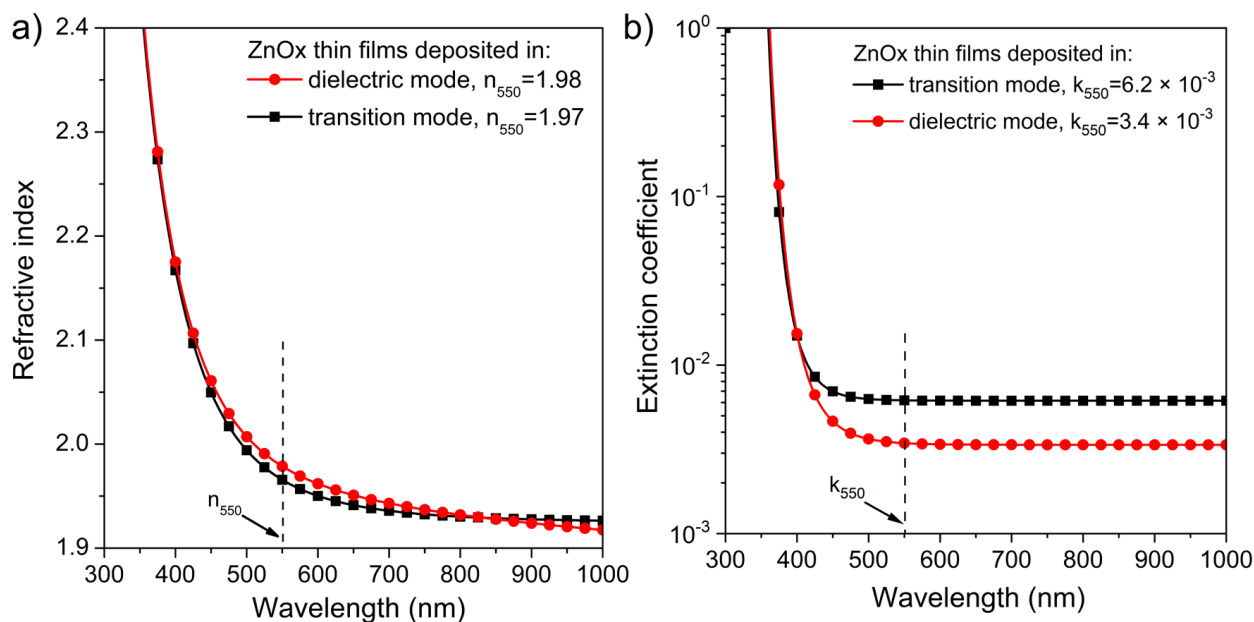


Figure 9. Spectral characteristics of: (a) refractive index and (b) extinction coefficient of transparent ZnOx thin films.

3.4. Electrical Properties of ZnOx Thin Films

Based on the current-voltage characteristics measured in a planar configuration, the values of sheet resistance (R_{sheet}) and resistivity (ρ) were determined. The resistivity of the nanocrystalline thin film deposited in metallic mode was equal to $3.8 \times 10^{-4} \Omega\text{cm}$, which clearly showed that the occurrence of the oxide ZnO-hexagonal phase in its structure did not cause a significant increase of ρ as compared to pure metallic Zn. For the prepared ZnO coatings in dielectric modes ($c1$; $c2$), the resistivity was equal to $3.2 \times 10^7 \Omega\text{cm}$ and $4.5 \times 10^8 \Omega\text{cm}$, respectively. The current-voltage characteristics for ZnOx thin films are presented in Figure 10. Based on these results, one can observe that different technological parameters of the pulsed reactive magnetron sputtering process had considerable influence on electrical parameters. The ZnOx thin films deposited with different partial pressure

of oxygen p_{O_2} at the (a) work point were significantly different compared to the films deposited at (c1) and (c2) work points.

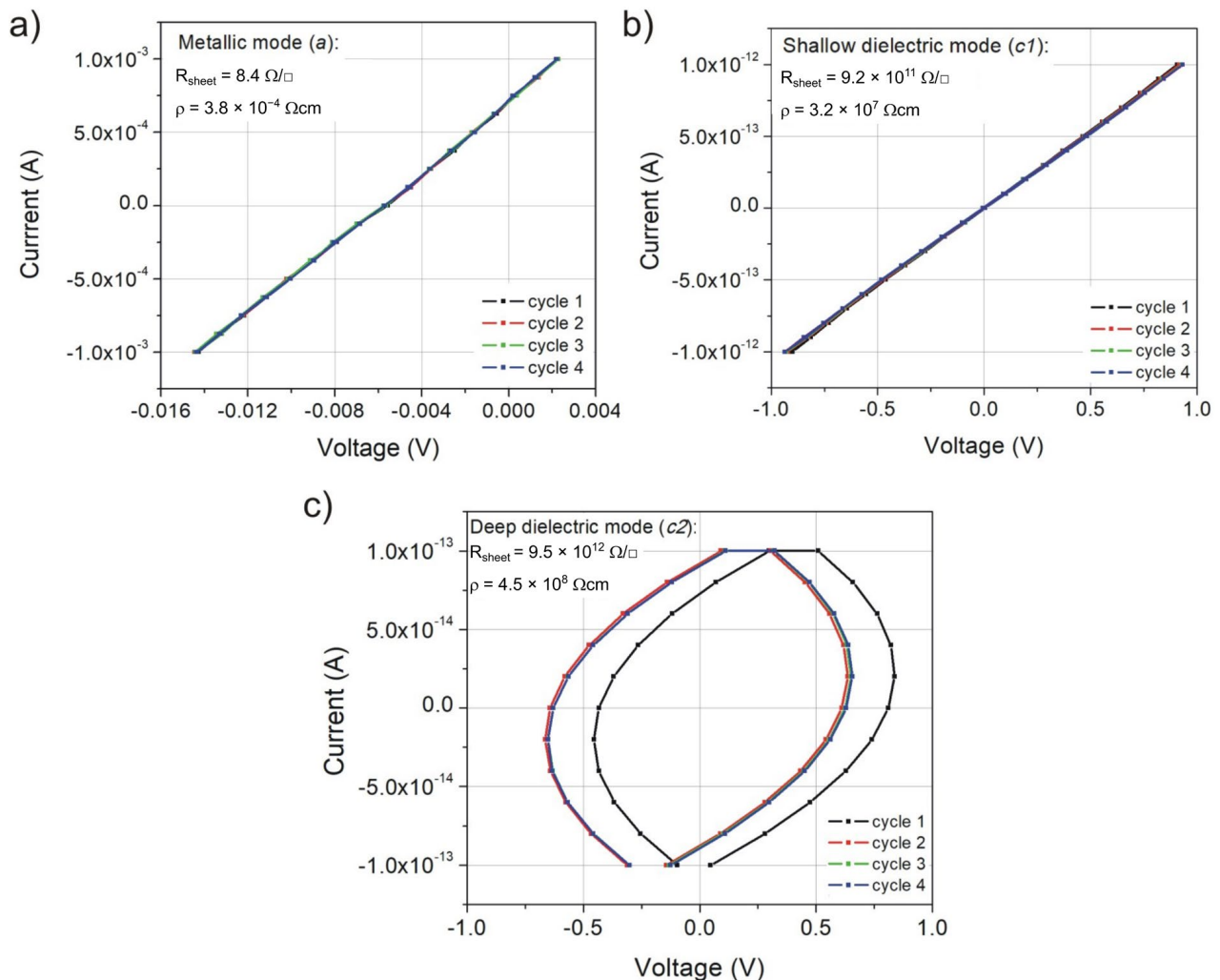


Figure 10. Current-voltage characteristics for ZnOx thin films deposited at modes: (a) metallic (a), (b) shallow dielectric (c1) and (c) deep dielectric (c2).

3.5. Mechanical Properties of ZnOx Thin Films

The results of the nanoindentation investigations of ZnOx thin films are shown in Figure 11. The hardness of the deposited coatings varied significantly between films deposited in different sputtering modes. The lowest hardness was obtained for ZnOx thin film deposited in the metallic mode. This could be anticipated due to the low hardness of metallic zinc whose hardness on the Mohs scale is only 2.5; therefore, it is the same as rather soft silver and magnesium and slightly harder than lead, known as a soft metal. In the case of the thin films deposited in the dielectric modes, their hardness was much higher and equal to 8.5 and 11.5 GPa for the film sputtered in a shallow and deep dielectric mode, respectively. The first value is consistent with the literature reports, where the hardness of ZnO thin films is usually in the range of 5 to 8 GPa. However, values as low as 2 GPa or as high as 10.8 GPa can also be found [52–62]. It is worth noting that the hardness obtained for ZnOx thin films sputtered in the deep dielectric mode was one of the highest in all of the literature reports to date. This might be caused by the highly nanocrystalline structure, where the crystallite size is only 8.1 nm. In the case of the ZnOx thin films deposited in shallow dielectric mode, the crystallite size is slightly larger and equal to 8.7 nm, which might be the reason for the lower hardness due to the Hall–Petch effect. However, both

thin films had a smooth surface with homogeneously distributed nanograins and exhibited a densely packed, void-free, nonporous columnar microstructure. The refractive index of the film prepared in the deep dielectric mode is slightly higher than that of the shallow dielectric mode. At $\lambda = 500$ nm, n is equal to 2.01 and 1.99 for deep and shallow dielectric modes, respectively. Both values are close to those of a single ZnO crystal, which is equal to 2.05 at the same wavelength [63]. Furthermore, both values are rather high compared to literature reports, where n is usually in the range of 1.9 to 2 [64–68]. On the basis of the values of the refractive index, the packing density of both thin films was determined according to the Equation (2) [69,70]:

$$P = \frac{(n_f^2 - 1) \cdot (n_b^2 + 1)}{(n_f^2 + 2) \cdot (n_b^2 - 1)} \quad (2)$$

where: n_f is the refractive index of ZnO thin films at 500 nm and n_b is the refractive index of bulk ZnO at 500 nm.

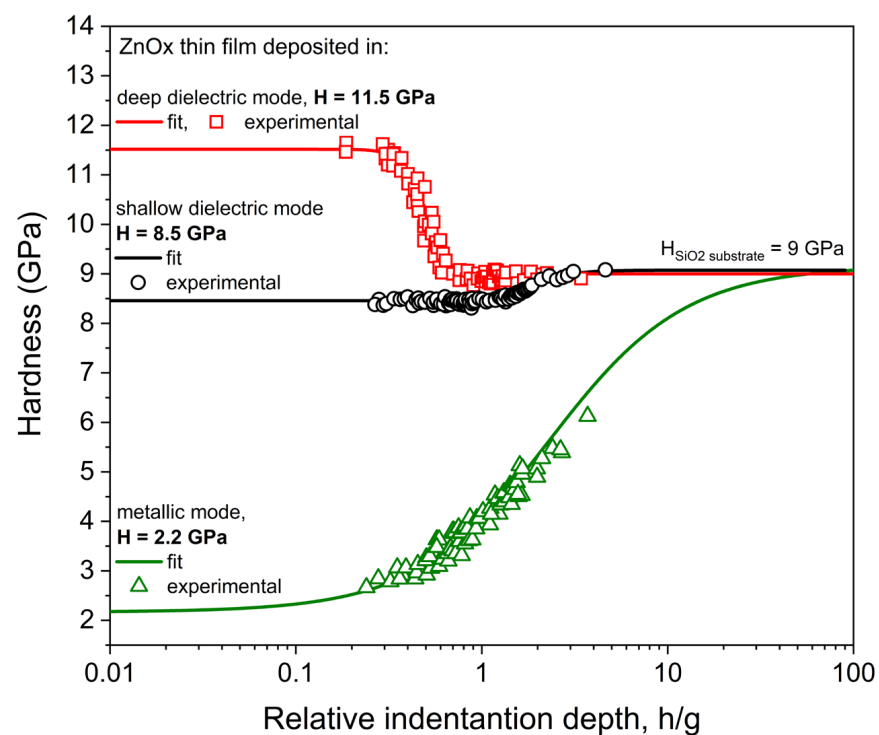


Figure 11. Results of hardness investigations of ZnOx thin films deposited with various technological parameters.

In this way, a direct comparison could be made between the deposited thin films. The better packing density was found for the ZnOx thin film prepared in the deep dielectric mode and was equal to 0.972 compared to 0.964 obtained for shallow dielectric mode conditions. These results are consistent with the hardness measurements and the crystallite size of both types of coatings.

Furthermore, the abrasion resistance of each deposited thin film was estimated based on the Bayer test. This parameter is especially important in the case of protective transparent coatings that may be applied in various fields of optics or optoelectronics, e.g., in ophthalmics or touch screens. The investigation results are shown in Figure 12. Each thin film was measured before and after performing the scratch test using an optical microscope working in reflection mode and an optical profilometer to obtain the 3D images of the surface and 2D surface cross-sectional profiles. Based on these data, surface roughness was determined using the root mean square height (Sq), and its change was used to evaluate

scratch resistance ($SRes$) (Equation (1)). Each sample had a homogeneous and crack-free surface before performing the scratch test, and the Sq value was in the range of 1.06 to 1.25 nm. After performing the Bayer test, the metallic coating was rough, containing visible scratch lines with a depth of even 400 nm. The Sq changed significantly and the $SRes$ value was only 1.64%, which clearly shows that this coating is not scratch resistant. In turn, both thin films sputtered in dielectric modes looked similar before and after the test. The 3D image of the surface and surface cross-section profile for thin films from the shallow dielectric mode showed some minor changes, while the Sq value increased slightly. Moreover, the optical microscope observations also showed some very small and difficult-to-see scratches. This resulted in a $SRes$ value of 78.9%, which indicates fairly good scratch resistance. However, the best ZnO thin films were deposited in the deep dielectric mode. The images of the optical microscope and profilometer did not show almost any change in the surface and Sq value after the Bayer test, resulting in a $SRes$ of 96.9%. This testifies about a very good scratch resistance of these coatings.

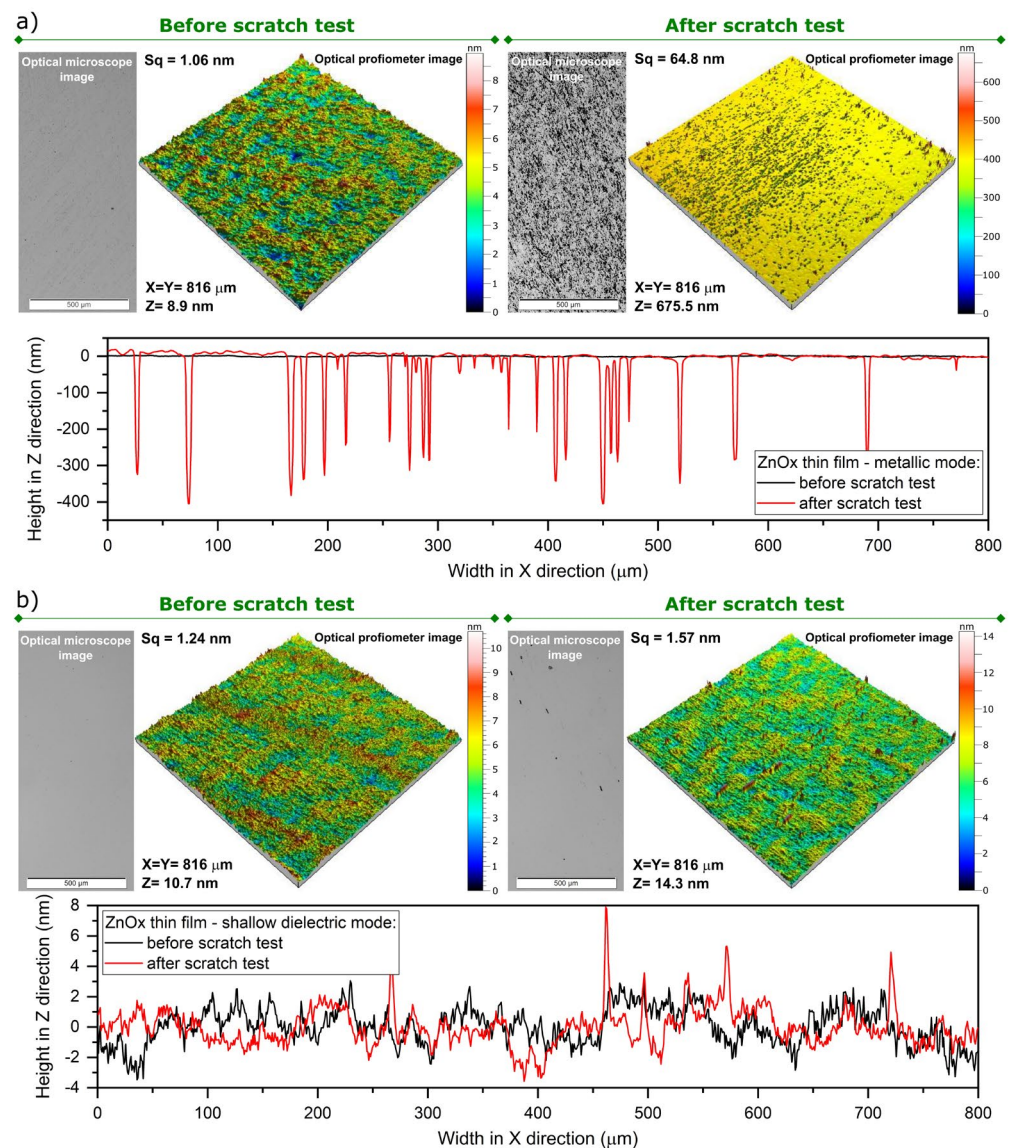


Figure 12. Cont.

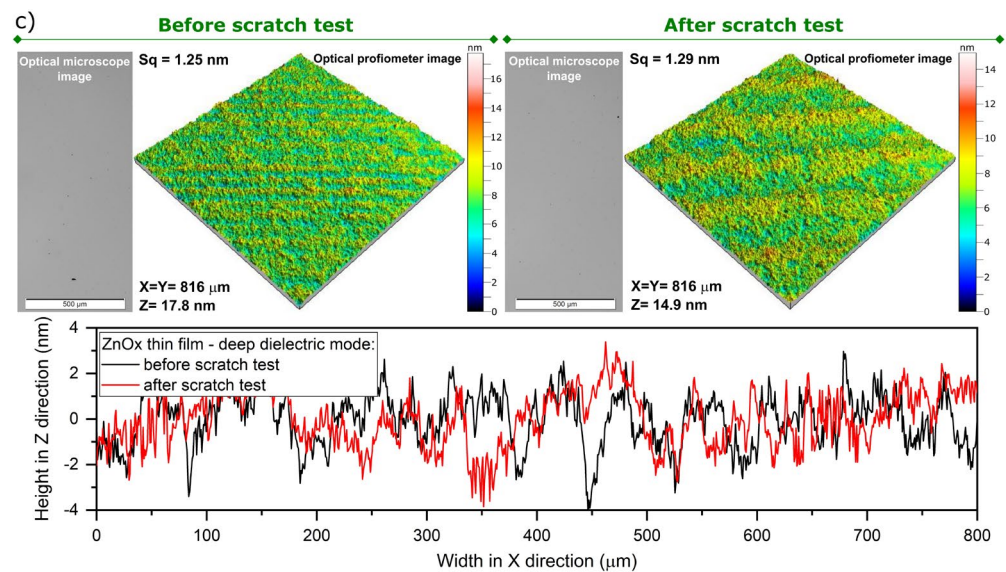


Figure 12. Optical microscope and profilometer images and surface cross-sectional profiles of ZnOx thin films deposited in various sputtering modes: (a) metallic, (b) shallow dielectric and (c) deep dielectric before and after performing abrasion tests.

Summary of the obtained results for ZnOx thin films is shown in Table 2.

Table 2. Summary of the results of investigations for ZnOx thin films.

ZnOx Thin Film—Deposition Mode	T_{λ} (%)	$\lambda_{\text{cut-off}}$ (nm)	n_{550}	k_{550}	R_{sheet} (Ω/\square)	ρ (Ωcm)	Hardness (Gpa)	SRes (%)
metallic	0	0	-	-	8.4	3.8×10^{-4}	2.2	1.64
shallow dielectric	84	361	1.97	6.2×10^{-3}	9.2×10^{11}	3.2×10^7	8.5	78.9
deep dielectric	84	370	1.98	3.4×10^{-3}	9.5×10^{12}	4.5×10^8	11.5	96.9

Designations: T_{λ} —transmittance, $\lambda_{\text{cut-off}}$ —fundamental absorption edge, n_{550} —refractive index at $\lambda = 550$ nm, k_{550} —extinction coefficient at $\lambda = 550$ nm, R —resistance, ρ —resistivity, S_{res} —scratch resistance according to (Equation (1)).

4. Conclusions

The ZnOx thin films were deposited with different oxygen concentrations in the sputtering atmosphere, which determined three different sputtering modes: metallic, shallow dielectric and deep dielectric modes. All prepared ZnOx films were obtained with a relatively high deposition rate, which was related to the high target power density during the sputtering process, which was not found in the other works. Microstructure studies showed that thin films deposited in the metallic mode had mixed metallic (Zn) and oxide (ZnO) hexagonal crystal phases with crystallite size of 9.1 and 6.0 nm, respectively. Moreover, thin films deposited in shallow and deep dielectric modes had a polycrystalline structure of the hexagonal ZnO phase with crystallite size of 8.1 to 8.7 nm. It was also found that coatings deposited in the metallic mode were opaque, which was related to the occurrence of metallic Zn in the deposited thin film. On the contrary, thin films deposited at shallow and dielectric modes were highly transparent, with an average transparency in the visible wavelength range above 84%. On the basis of the extinction coefficient values, it can be concluded that the optical losses are almost two times smaller for ZnOx coatings deposited in the deep dielectric mode compared to films deposited in the shallow dielectric mode. Measurements of electrical properties revealed that the resistivity of as-deposited thin films was dependent on the sputtering mode. For coatings deposited in the metallic mode, the resistivity was equal to $3.8 \times 10^{-4} \Omega\text{cm}$, while for films deposited in the dielectric modes, it was significantly higher and was in the range from 10^7 to $10^8 \Omega\text{cm}$.

Measurements of nanomechanical properties revealed that metallic thin films were rather soft with hardness of 2.2 GPa, but it is worth mentioning that coatings from the deep dielectric mode had one of the highest values of hardness ever reported, i.e., 11.5 Gpa. Moreover, coatings deposited in the dielectric modes were scratch resistant, and the best abrasive properties were obtained for the ZnO thin film prepared in deep dielectric mode.

Author Contributions: Conceptualization, M.M., A.O. and W.P.; methodology, M.M., A.O., S.K. and W.P.; validation, M.M., W.P., D.W. and J.D.; formal analysis, M.M., A.O., M.K., M.G. and W.P.; investigation, M.M., A.O., W.P., S.K., A.W., D.W., J.D., M.K., M.G. and J.S.; resources, M.M. and J.D.; data curation, M.M. and A.O.; writing—original draft preparation, M.M., A.O. and W.P.; writing—review and editing, M.M. and J.D.; visualization, M.M., A.O. and W.P.; supervision, M.M.; project administration, M.M.; funding acquisition, M.M. and J.S. All authors have read and agreed to the published version of the manuscript.

Funding: This work was co-funded within the project No UMO-2020/39/D/ST5/00424 from the Polish National Science Centre in the years 2021–2024.

Institutional Review Board Statement: Not applicable.

Informed Consent Statement: Not applicable.

Data Availability Statement: The data presented in this study are available on request from the corresponding author via e-mail.

Conflicts of Interest: The authors declare no conflict of interest.

References

1. Muchuweni, E.; Sathiaraj, T.S.; Nyakoty, H. Synthesis and characterization of zinc oxide thin films for optoelectronic applications. *Heliyon* **2017**, *3*, e00285. [[CrossRef](#)] [[PubMed](#)]
2. Dave, P.Y.; Patel, K.H.; Chauhan, K.V.; Chawla, A.K.; Rawal, S.K. Examination of zinc oxide films prepared by magnetron sputtering. *Proc. Tech.* **2016**, *23*, 328–335. [[CrossRef](#)]
3. Ismail, A.; Abdullah, M.J. The structural and optical properties of ZnO thin films prepared at different RF sputtering power. *J. King Saud Univ. Sci.* **2013**, *25*, 209–215. [[CrossRef](#)]
4. Viswanathan, K.; Shyju, T.S.; Ramachandran, D.; Pradhaban, G. Electric properties of ZnO thin films by RF magnetron sputtering technique. *Mater. Today-Proc.* **2016**, *3*, 1548–1552. [[CrossRef](#)]
5. Bedia, A.; Bedia, F.Z.; Aillerie, M.; Maloufi, N.; Benyoucef, B. Morphological and optical properties of ZnO thin films prepared by spray pyrolysis on glass substrates at various temperatures for integration in solar cell. *Energy Proced.* **2015**, *74*, 529–538. [[CrossRef](#)]
6. Axelevitch, A.; Gorenstein, B.; Darawshe, H.; Golan, G. Investigation of thin solid ZnO films prepared by sputtering. *Thin Solid Film.* **2010**, *518*, 4520–4524. [[CrossRef](#)]
7. Vemuri, S.K.; Khanna, S.; Paneliya, S.; Takhar, V.; Banerjee, R.; Mukhopadhyay, I. Fabrication of silver nanodome embedded zinc oxide nanorods for enhanced Raman spectroscopy. *Colloids Surf. A* **2022**, *639*, 128336. [[CrossRef](#)]
8. Wang, F.H.; Chen, M.S.; Liu, H.W.; Kang, T.K. Effect of rapid thermal annealing time on ZnO:F thin films deposited by radio frequency magnetron sputtering for solar cell applications. *Appl. Phys. A* **2022**, *128*, 227. [[CrossRef](#)]
9. Wójcicka, A.; Fogarassy, Z.; Rącz, A.; Kravchuk, T.; Sobczak, G.; Borysiewicz, M.A. Multifactorial investigations of the deposition process—Material property relationships of ZnO: Al thin films deposited by magnetron sputtering in pulsed DC, DC and RF modes using different targets for low resistance highly transparent films on unheated substrates. *Vacuum* **2022**, *203*, 111299. [[CrossRef](#)]
10. Kołodziejczak-Radzimska, A.; Jesionowski, T. Zinc oxide—From synthesis to application: A review. *Materials* **2014**, *7*, 2833–2881. [[CrossRef](#)]
11. Rajalakshmi, R.; Angappane, S. Effect of thickness on the structural and optical properties of sputtered ZnO and ZnO: Mn thin films. *J. Alloys Compd.* **2014**, *615*, 355–362. [[CrossRef](#)]
12. Hussain, S.; Liu, T.; Kashif, M.; Miao, B.; He, J.; Zeng, W.; Zhang, Y.; Hasim, U.; Fusheng, P. Surfactant dependent growth of twinned ZnO nanodisks. *Mater. Lett.* **2014**, *118*, 165–168. [[CrossRef](#)]
13. Kim, J.H.; Do, K.M.; Kim, J.W.; Jung, J.C.; Lee, J.H.; Moon, B.M.; Koo, S.M. Fabrication and characterization of nanocrystalline ZnO film-based heterojunction diodes on 4H-SiC. *J. Nanoelectr. Optoelectr.* **2012**, *7*, 271–274. [[CrossRef](#)]
14. Varma, T.; Sharma, S.; Periasamy, C.; Boolchandani, D. Performance analysis of Pt/ZnO schottky photodiode using ATLAS. *J. Nanoelectr. Optoelectr.* **2015**, *10*, 761–765. [[CrossRef](#)]
15. Lee, B.S.; Joo, Y.H.; Kim, C.I. The optical and electrical characteristics for ZnO/Al/ZnO multilayer films deposited by RF sputtering. *J. Nanoelectr. Optoelectr.* **2015**, *1*, 402–407. [[CrossRef](#)]

16. Chaari, M.; Matoussi, A. Electrical conduction and dielectric studies of ZnO pellets. *Phys. B Condens. Mater.* **2012**, *407*, 3441–3447. [[CrossRef](#)]
17. Liu, H.; Yang, D.; Yang, H.; Zhang, H.; Zhang, W.; Fang, Y.; Liu, Z.; Tian, L.; Lin, B.; Yan, J.; et al. Comparative study of respiratory tract immune toxicity induced by three sterilization nanoparticles: Silver, zinc oxide and titanium dioxide. *J. Hazard. Mater.* **2013**, *248*, 478–486. [[CrossRef](#)]
18. O'Brien, S.; Nolan, M.G.; Çopuroglu, M.; Hamilton, J.A.; Povey, I.; Pereira, L.; Martins, R.; Fortunato, E.; Pemble, M. Zinc oxide thin films: Characterization and potential applications. *Thin Solid Film.* **2010**, *518*, 4515–4519. [[CrossRef](#)]
19. Kadem, B.; Banimuslem, H.A.; Hassan, A. Modification of morphological and optical properties of ZnO thin film. *Karbala Int. J. Mod. Sci.* **2017**, *3*, 103–110. [[CrossRef](#)]
20. Yamamoto, T.; Shiosaki, T.; Kawabata, A. Characterization of ZnO piezoelectric films prepared by rf planar-magnetron sputtering. *J. Appl. Phys.* **1980**, *51*, 3113–3120. [[CrossRef](#)]
21. Krupanidhi, S.B.; Sayer, M. Position and pressure effects in rf magnetron reactive sputter deposition of piezoelectric zinc oxide. *J. Appl. Phys.* **1984**, *56*, 3308–3318. [[CrossRef](#)]
22. Sundaram, K.B.; Garside, B.K. Properties of ZnO films reactively RE sputtered using a Zn target. *J. Phys. D Appl. Phys.* **1984**, *17*, 147–153. [[CrossRef](#)]
23. Srivastav, S.; Vasant Kumar, C.V.R.; Mansingh, A. Effect of oxygen on the physical parameters of RF sputtered ZnO thin film. *J. Phys. D Appl. Phys.* **1989**, *22*, 1768–1772. [[CrossRef](#)]
24. Tsuji, N.; Komiya, H.; Tanaka, K. Growth mechanism of ZnO film by reactive sputtering method—Significance of thermodynamics in a plasma system. *Jpn. J. Appl. Phys.* **1990**, *29*, 835–841. [[CrossRef](#)]
25. Fang, Z.; Wang, Y.; Peng, X.; Liu, X.; Zhen, C. Structural and optical properties of ZnO films grown on the AAO templates. *Mater. Lett.* **2003**, *57*, 4187–4190. [[CrossRef](#)]
26. Ondo-Ndong, R.; Pascal-Delannoy, F.; Boyer, A.; Giani, A.; Foucaran, A. Structural properties of zinc oxide thin films prepared by r.f. magnetron sputtering. *Mater. Sci. Eng. B* **2003**, *97*, 68–73. [[CrossRef](#)]
27. Yasui, K.; Phuong, N.V.; Kuroki, Y.; Takata, M.; Akahane, T. Improvement in crystallinity of ZnO films prepared by rf magnetron sputtering with grid electrode. *Jpn. J. Appl. Phys.* **2005**, *44*, 684–687. [[CrossRef](#)]
28. Choongmo, K.; Sookjoo, K.; Chongmu, L. Effects of RF power and substrate temperature during RF magnetron sputtering on crystal quality of ZnO thin films. *Jpn. J. Appl. Phys.* **2005**, *44*, 8501–8503. [[CrossRef](#)]
29. Ye, J.Y.; Huang, Z.Y.; Min, C.; Pan, S.R.; Chen, D.H. Structure and haemocompatibility of ZnO films deposited by radio frequency sputtering. *Biomed. Mater.* **2009**, *4*, 055004. [[CrossRef](#)]
30. Ghosh, S.P.; Das, K.C.; Tripathy, N.; Bose, G.; Lee, T.; Myoung, J.M.; Kar, J.P. Morphological and photoluminescence analysis of zinc oxide thin films deposited by RF sputtering at different substrate temperatures. *IOP Conf. Ser. Mater. Sci. Eng.* **2015**, *75*, 012023. [[CrossRef](#)]
31. Gonçalves, R.S.; Barrozo, P.; Cunha, F. Optical and structural properties of ZnO thin films grown by magnetron sputtering: Effect of the radio frequency power. *Thin Solid Film.* **2016**, *616*, 265–269. [[CrossRef](#)]
32. Acosta, M.; Riech, I.; Martín-Tova, E. Effects of the argon pressure on the optical band gap of zinc oxide thin films grown by nonreactive RF sputtering. *Adv. Cond. Matter Phys.* **2013**, *2013*, 970976. [[CrossRef](#)]
33. Hata, T.; Minamikawa, T.; Noda, E.; Morimoto, O.; Hada, T. High rate deposition of ZnO film using improved DC reactive magnetron sputtering technique. *Jpn. J. Appl. Phys.* **1979**, *18*, 219–224. [[CrossRef](#)]
34. Hata, T.; Takeda, F.; Morimoto, O.; Noda, E.; Hada, T. High rate deposition of thick piezoelectric ZnO and AlN films using a new magnetron sputtering technique. *Jpn. J. Appl. Phys.* **1981**, *20*, 145–148. [[CrossRef](#)]
35. Chen, J.J.; Gao, Y.; Zeng, F.; Li, D.M.; Pan, F. Effect of sputtering oxygen partial pressures on structure and physical properties of high resistivity ZnO films. *Appl. Surf. Sci.* **2004**, *223*, 318–329. [[CrossRef](#)]
36. Czternastek, H. ZnO thin films prepared by high pressure magnetron sputtering. *Opto-Electron. Rev.* **2004**, *12*, 49–52.
37. Samarasekera, P.; Yapa, N.U.S.; Kumara, N.T.R.N.; Perera, M.V.K. CO₂ gas sensitivity of sputtered zinc oxide thin films. *Bull. Mater. Sci.* **2007**, *30*, 113–116. [[CrossRef](#)]
38. Hezam, M.; Tabet, N.; Mekki, A. Synthesis and characterization of DC magnetron sputtered ZnO thin films under high working pressures. *Thin Solid Film.* **2010**, *518*, 161–164. [[CrossRef](#)]
39. Welzel, T.; Ellmer, K. Negative oxygen ion formation in reactive magnetron sputtering processes for transparent conductive oxides. *J. Vac. Sci. Technol. A* **2012**, *30*, 061306. [[CrossRef](#)]
40. Masłyk, M.; Borysiewicz, M.A.; Wzorek, M.; Wojciechowski, T.; Kwoka, M.; Kaminska, E. Influence of absolute argon and oxygen flow values at a constant ratio on the growth of Zn/ZnO nanostructures obtained by DC reactive magnetron sputtering. *Appl. Surf. Sci.* **2016**, *389*, 287–293. [[CrossRef](#)]
41. Kwoka, M.; Lyson-Sypien, B.; Kulis, A.; Masłyk, M.; Borysiewicz, M.A.; Kaminska, E.; Szuber, J. Surface properties of nanostructured, porous ZnO thin films prepared by direct current reactive magnetron sputtering. *Materials* **2018**, *11*, 131. [[CrossRef](#)]
42. Tominaga, K.; Yuasa, T.; Kume, M.; Tada, O. Influence of energetic oxygen bombardment on conductive ZnO film. *Jpn. J. Appl. Phys.* **1985**, *24*, 944–949. [[CrossRef](#)]
43. Tominaga, K.; Kume, M.; Yuasand, T.; Tada, O. High-energy oxygen atoms in ZnO film preparation by reactive sputtering of Zn. *Jpn. J. Appl. Phys.* **1985**, *24*, 28–30. [[CrossRef](#)]

44. Konstantinidis, S.; Hemberg, A.; Dauchot, J.P.; Hecq, M. Deposition of zinc oxide layers by high-power impulse magnetron sputtering. *J. Vac. Sci. Technol. B* **2007**, *25*, L19–L21. [[CrossRef](#)]
45. Partridge, J.G.; Mayes, E.L.H.; McDougall, N.L.; Bilek, M.M.M.; McCulloch, D.G. Characterization and device applications of ZnO films deposited by high power impulse magnetron sputtering (HiPIMS). *J. Phys. D Appl. Phys.* **2013**, *46*, 165105. [[CrossRef](#)]
46. Reed, A.N.; Shamberger, P.J.; Hu, J.J.; Muratore, C.; Bultman, J.E.; Voevodin, A.A. Microstructure of ZnO thin films deposited by high power impulse magnetron sputtering. *Thin Solid Film.* **2015**, *579*, 30–37. [[CrossRef](#)]
47. Posadowski, W.; Wiatrowski, A.; Dora, J.; Radzimski, Z. Magnetron sputtering process control by medium-frequency power supply parameter. *Thin Solid Film.* **2008**, *516*, 4478–4482. [[CrossRef](#)]
48. Klug, H.P.; Alexander, L.E. *X-ray Diffraction Procedures for Polycrystalline and Amorphous Materials*, 2nd ed.; John Wiley and Sons: New York, NY, USA, 1974; p. 8.
49. Oliver, W.C.; Pharr, G.M. An improved technique for determining hardness and elastic modulus using load and displacement sensing indentation experiments. *J. Mater. Res.* **1992**, *7*, 1564–1583. [[CrossRef](#)]
50. *Standard Test Method for Abrasion Resistance of Transparent Plastics and Coatings Using the Oscillating Sand Method*; ASTM International: West Conshohocken, PA, USA, 2017.
51. Tauc, J. *Amorphous and Liquid Semiconductor*; Plenum Press: New York, NY, USA, 1974; p. 159.
52. Zheng, X.; Yan, D.; Yi, C.; Zhu, J.; Zhang, Q.; Zhai, J.; Ma, T.; Zhu, P.; Li, H.; Gu, L.; et al. The discovery of a superhard P-type transparent semiconductor: Al_{2.69}B₅₀. *Mater. Horiz.* **2022**, *9*, 748–755. [[CrossRef](#)]
53. Yonemura, I. Thermo-mechanical stability of wide-bandgap semiconductors: High temperature hardness of SiC, AlN, GaN, ZnO and ZnSe. *Phys. B* **2001**, *308–310*, 1150–1152. [[CrossRef](#)]
54. Lee, K.H. Semi-transparent organic/inorganic hybrid photo-detector using pentacene/ZnO diode connected to pentacene transistor. *Org. Electron.* **2011**, *12*, 1103–1107. [[CrossRef](#)]
55. Zhao, S.; Zhou, Y.; Liu, Y.; Zhao, K.; Wang, S.; Xiang, W.; Liu, Z.; Han, P.; Chen, Z.; Lu, H.; et al. Enhanced hardness in B-doped ZnO thin films on fused quartz substrates by pulsed-laser deposition. *Appl. Surf. Sci.* **2006**, *253*, 726–729. [[CrossRef](#)]
56. Roy, T.K. Assessing hardness and fracture toughness in sintered zinc oxide ceramics through indentation technique. *Mat. Sci. Eng. A-Struct.* **2015**, *640*, 267–274. [[CrossRef](#)]
57. Bhardwaj, V.; Chowdhury, R.; Jayaganthan, R. Nanomechanical and microstructural characterization of sputter deposited ZnO thin films. *Appl. Surf. Sci.* **2016**, *389*, 1023–1032. [[CrossRef](#)]
58. Yen, C.Y.; Jian, S.R.; Chen, G.J.; Lin, C.M.; Lee, H.Y.; Ke, W.C.; Liao, Y.; Yang, P.-F.; Wang, C.-T.; Lai, Y.-S.; et al. Influence of annealing temperature on the structural, optical and mechanical properties of ALD-derived ZnO thin films. *Appl. Surf. Sci.* **2011**, *257*, 7900–7905. [[CrossRef](#)]
59. Pat, S.; Mohammadigharehbagh, R.; Ozen, S.; Senay, V.; Yudar, H.H.; Korkmaz, S. The Al doping effect on the surface, optical, electrical and nanomechanical properties of the ZnO and AZO thin films prepared by RF sputtering technique. *Vacuum* **2017**, *141*, 210–215. [[CrossRef](#)]
60. Jian, S.R.; Chen, H.G.; Chen, G.J.; Jang, J.S.C.; Juang, J.Y. Structural and nanomechanical properties of a-plane ZnO thin films deposited under different oxygen partial pressures. *Curr. Appl. Phys.* **2012**, *12*, 849–853. [[CrossRef](#)]
61. Jian, S.R.; Chen, G.J.; Wang, S.K.; Lin, T.C.; Jang, J.S.C.; Juang, J.Y.; Lai, Y.S.; Tseng, J.Y. Rapid thermal annealing effects on the structural and nanomechanical properties of Ga-doped ZnO thin films. *Surf. Coat. Technol.* **2013**, *231*, 176–179. [[CrossRef](#)]
62. Boryło, P.; Matus, K.; Lukaszewicz, K.; Kubacki, J.; Balin, K.; Basiaga, M.; Szindler, M.; Mikula, J. The influence of atomic layer deposition process temperature on ZnO thin film structure. *Appl. Surf. Sci.* **2019**, *474*, 177–186. [[CrossRef](#)]
63. Bond, W.L. Measurement of the refractive indices of several crystals. *J. Appl. Phys.* **1965**, *36*, 1674–1677. [[CrossRef](#)]
64. Al-Kuhaili, M.F.; Durrani, S.M.A.; El-Said, A.S.; Heller, R. Enhancement of the refractive index of sputtered zinc oxide thin films through doping with Fe₂O₃. *J. Alloys Compd.* **2017**, *690*, 453–460. [[CrossRef](#)]
65. Cetinorgu, E.; Goldsmith, S.; Boxman, R.I. The effect of substrate temperature on filtered vacuum arc deposited zinc oxide and tin oxide thin films. *J. Cryst. Growth* **2007**, *299*, 259–267. [[CrossRef](#)]
66. Gupta, V.; Mansingh, A. Influence of postdeposition annealing on the structural and optical properties of sputtered zinc oxide film. *J. Appl. Phys.* **1996**, *80*, 1063–1073. [[CrossRef](#)]
67. Dumont, E.; Dugnoille, B.; Bienfait, S. Simultaneous determination of the optical properties and of the structure of r.f.-sputtered ZnO thin films. *Thin Solid Film.* **1999**, *353*, 93–99. [[CrossRef](#)]
68. Kang, S.J.; Joung, Y.H. Influence of substrate temperature on the optical and piezoelectric properties of ZnO thin films deposited by rf magnetron sputtering. *Appl. Surf. Sci.* **2007**, *253*, 7330–7335. [[CrossRef](#)]
69. Dave, V.; Dubey, P.; Gupta, H.O.; Chandra, R. Influence of sputtering pressure on the structural, optical and hydrophobic properties of sputtered deposited HfO₂ coatings. *Thin Solid Film.* **2013**, *549*, 2–7. [[CrossRef](#)]
70. Bauer, G. Absolutwerte der optischen Absorptionskonstanten von Alkalihalogenidkristallen im Gebiet ihrer ultravioletten Eigenfrequenzen. *Ann. Phys.* **1934**, *411*, 434–464. [[CrossRef](#)]